POLISH MARITIME RESEARCH 1 (121) 2024 Vol. 31; pp. 55-63
10.2478/pomr-2024-0006

UNIVERSAL SEA/FEM BASED METHOD FOR ESTIMATION OF VIBROACOUSTIC COUPLING LOSS FACTORS IN REALISTIC SHIP STRUCTURES

Michał Drężek*
[1] Fem4cad Sp. z o.o, Gdynia,
[2] Gdańsk University of Technology, Industrial Doctoral School,Gdańsk, Gdańsk, Poland,
Marek Augustyniak
Gdansk University of Technology, Institute of Nanotechnology and Materials Engineering, Poland

* Corresponding author: *michaldrezek@gmail.com (Michał Drężek)*

ABSTRACT

Despite the fact that there is an existing body of literature addressing the computation of Coupling Loss Factors (CLFs) via the Finite Element Method (FEM), no publications have sufficiently taken into account real structural joints in their approach. Previous research has focused on academic cases of trivial connections, rarely involving more than two steel plates. To enable Statistical Energy Analysis (SEA) on a real ship, a methodology for determining CLFs for non-trivial systems is proposed, considering realistic boundary conditions and irregularities that can occur in marine structures. Based on the method, a library of CLFs is created by selecting the tested connections to enable modelling of about 90% of the acoustic paths on an existing jack-up vessel. Boundary conditions were set by introducing spring elements with a stiffness calibrated to the type of connection and taking the adjacent structure into account. In previous works, CLFs were determined for basic connections of rectangular plates. The lack of scantling variations, ignoring discontinuities and only defining parallel edges in the considered models, lead to the overestimation of energy transmission in real structures. To consider the influence of the above, random deviations from the initial stiffness of the springs at individual edges and point restraints at random points are introduced in this paper.

Keywords: Statistical Energy Analysis, Power Injection Method, Finite Element Method, Coupling Loss Factor

INTRODUCTION

Passenger ships, commercial ships and specialised vessels are treated as ordinary workplaces, with respect to vibroacoustic conditions, although they have their own unique character, being places of both professional and leisure activities [1]. For their health, it is important to reduce the levels of daily noise and vibration to which they are exposed. To do this, one has to be able to predict the transmission of vibroacoustic energy at the design stage. Energy-based modelling approaches are often used to describe the higher frequency vibrational behaviour of complex systems in some average, statistical or approximate way. The most important of these methods is statistical energy analysis (SEA). At low frequencies, the finite element method (FEM) is used. This article focuses on determining coupling loss factors (CLF) for real-world structural connections in the medium and high frequencies (octaves 63-2000 Hz). CLFs are key parameters for SEA; they describe the energy transmission between connected subsystems.

BASICS OF SEA

SEA involves the prediction of the vibration response of a complex structure by dividing it into subsystems and determining the average energy. The transmission of vibration energy between subsystems is characterised by damping loss factors (DLF) and coupling loss factors (CLF). The DLF corresponds to the damping in the subsystem itself and the CLF corresponds to the energy dissipation at the subsystem connections. The CLFs and the DLFs form a matrix of coefficients in the energy balance equation, which is used to calculate the energy of subsystems when the input powers are known. The CLFs can be obtained using an analytical wave approach for several types of junctions of semi-infinite plates. An alternative is the power injection method (PIM), which is an approach in which the CLF values can be obtained by measuring subsystem energy and power input [2].

The fundamental relationship, on which the SEA and PIM is based, is the balance between the input power and the output power of the subsystem (a part of the whole system e.g. a single wall). For the i-th subsystem, this equation has the following form:

$$P_{i,in} = P_{i,out} \tag{1}$$

$$P_{i,in} = P_{i,dissipated} + \sum_{j \neq i}^{N} P_{ij} \tag{2}$$

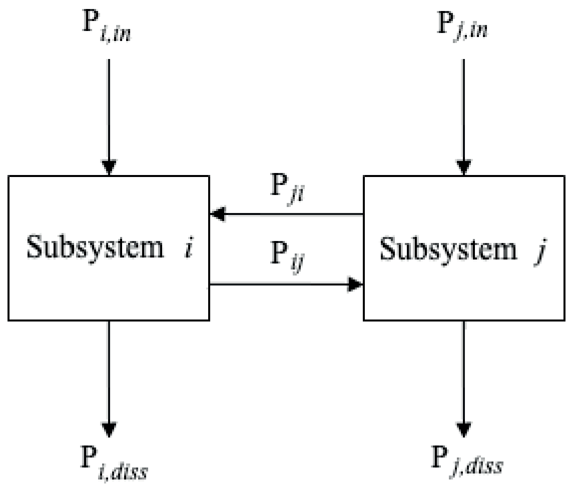

Fig. 1. Scheme of energy exchange in the SEA system

where $\sum_{j \neq i}^{N} P_{ij}$ is the power transferred by the i th subsystem to the subsystems coupled with it. It is assumed that there is no indirect coupling of subsystem s (only subsystems in the immediate vicinity can transfer energy to each other). The power dissipated by the subsystem depends on the damping loss factor and is calculated as follows:

$$P_{i,diss} = \omega \cdot \eta_i \cdot E_{i,tot} \tag{3}$$

where:
ω – the angular frequency corresponding to the centre frequency *f* of the band
η_i – damping loss factor (DLF)
$E_{i,tot}$ – total energy of the subsystem

The power transferred from subsystem i to subsystem j depends on the difference in vibration energy between them and can be represented by the following relationship:

$$P_{ij} = \omega \cdot \eta_{ij} \cdot E_{i,tot} - \omega \cdot \eta_{ij} \cdot E_{i,tot} \tag{4}$$

n_{ij} and n_{ji} are coupling loss factors (CLF) which are essential coefficients in SEA.

By knowing the above dependencies, it is possible to compose SEA equations, which can be presented in matrix form:

$$\omega \begin{vmatrix} \eta_i + \sum_{i \neq 1}^{N} \eta_{1i} & \cdots & -\eta_{1N} \\ \vdots & \ddots & \vdots \\ -\eta_{N1} & \cdots & \eta_N + \sum_{i \neq N}^{N-1} \eta_{Ni} \end{vmatrix} \times \begin{vmatrix} \langle E_1 \rangle \\ \vdots \\ \langle E_N \rangle \end{vmatrix} = \begin{vmatrix} P_{i,1} \\ \vdots \\ P_{i,N} \end{vmatrix} \tag{5}$$

The power injection method (sometimes called the experimental SEA or ESEA) involves exciting successive subsystems one by one with known power, measuring the total energies of the subsystems, and filling in the energy and power matrix. After inverting the energy matrix, a matrix of coefficients is obtained, according to the equation:

$$\omega \begin{vmatrix} \eta_i + \sum_{i \neq 1}^{N} \eta_{1i} & \cdots & -\eta_{1N} \\ \vdots & \ddots & \vdots \\ -\eta_{N1} & \cdots & \eta_N + \sum_{i \neq N}^{N-1} \eta_{Ni} \end{vmatrix} = \begin{vmatrix} P_1 & \cdots & 0 \\ \vdots & \ddots & \vdots \\ 0 & \cdots & P_N \end{vmatrix} \times \begin{vmatrix} \langle E_{11} \rangle & \cdots & \langle E_{N1} \rangle \\ \vdots & \ddots & \vdots \\ \langle E_{1N} \rangle & \cdots & \langle E_{NN} \rangle \end{vmatrix}^{-1} \tag{6}$$

In practice, both the total energy and input power values are difficult to obtain and are potential sources of inaccuracy. Moreover, creating a classic laboratory measuring system is costly and time-consuming. Therefore, methods using FEM are developed in parallel to experimental research.

STATE OF THE ART

The basics of both SEA and PIM are well described in the literature and yet some of their practical aspects remain challenging.

Le Bot and Cotoni [3] created validity diagrams of the SEA and described its assumptions in detail. The possibility of using PIM was indicated by Lyon as early as 1975 [4]. Laboratory experiments using this method have been described many times [5-7]. Due to the difficulty of controlling the input power and obtaining the energy of the subsystems, as well as the cost of both the measurement system and the test object, all of these tests were carried out for trivial systems. Numerical methods, in the form of a finite element method, became the next step in the development of PIM.

Pankaj et al. [8] described a method to carry out PIM using FEM. The expected results were obtained for an L-type connection for discrete frequencies. For SEA to be useful in industry, the coefficients must be averaged over the frequency domain. Only the simplest system was tested, i.e. two identical perpendicular plates. In a precisely uniform rectangular plate, the waves generated within the source plate propagate consistently along fixed paths, exhibiting no dispersion to alternate positions as they travel towards the receiving plate. This characteristic behaviour arises due to the absence of internal discontinuities and parallel sides. Such situations rarely occur in real structures. Even in ships built of repetitive structures, there are scantling variations, discontinuities and non-parallel edges. As a result, an irregular system has a smaller overall energy transmission than a regular system.

An interesting approach to estimating CLFs was presented by Thite and Mace [9], who proposed to randomise the properties of the system being analysed and average the resulting estimates but without repeating the full FEA. This allows for very computationally cheap results but is difficult to use in shipbuilding practice. The authors relied on the assumption that "response statistics are somewhat independent of detailed physical variables if the variability is 'large enough'". Unfortunately, in the case of ship's structures, the variability of physical properties is often not large enough, considering the criteria they adopt.

Poblet-Puig [10] developed a strategy to solve the problem of negative CLF values, which are sometimes obtained from Eq. (8). In the case of the structures considered in this article (due to their size), negative CLFs are rare and the proposed averaging technique allows them to be ignored.

There are also numerous publications on vibroacoustic transmission that use techniques other than PIM. Shorter and Langley [11] proposed a general method for predicting the ensemble average steady-state response of vibroacoustic systems. The authors not only decided not to recure to PIM, but bypassed the basic assumptions of SEA as well, concerning the strength of the coupling between the subsystems, the nature of the excitation, or the resonant nature of the response. Their approach also yielded 'indirect' CLFs (CLFs between statistical subsystems that are not physically adjacent).

Attempts to include stiffened plates in the framework of Statistical Energy Analysis have led to the creation of a new branch of SEA development, in which subsystems are treated as periodic structures. Yin and Hopkins [12] described the combination of Bloch theory and wave theory, while Pany [13] presented the combination of FEM with Floquet's theory. The asymmetrical stiffeners found in shipbuilding were not taken into account in any of these cases. The methods mentioned, ingenious as they are in some theoretical respects, remain insufficient for grasping the complexity of typical ship structures, featuring asymmetries, stiffeners and discontinuities.

Using these methods can be helpful but they are insufficient for ship construction, specifically.

The original contributions of the present research are:

- A library of SEA parameters is created for the structural joints of a jack-up vessel; by using this library, one can create many SEA models of vibroacoustic paths on various ships.
- The well-described PIM method is modified to easily reject negative CLFs with a minimal impact on the final result. The coefficients are averaged, both in the frequency domain and for various boundary conditions.
- A method of setting boundary conditions is proposed to take into account the influence of the adjacent structure and internal discontinuities.

NUMERICAL EXPERIMENTS

THE SELECTION OF STRUCTURAL CONNECTIONS

The structural connections shown in this article are parts of an existing jack-up vessel. They were selected based on the possibility of carrying out an SEA analysis for this unit. Using these specific cases, real vibroacoustic transmission paths can be modelled for many ships. Structural elements were 'cut out' from a global FEM model created for strength analyses. The global model is shown in Fig. 2. The mesh of finite elements was refined to meet the condition λ>7l for the selected submodels, where λ is the wavelength and l is the element length. This condition was introduced to make sure that the flexural wave was mapped correctly.

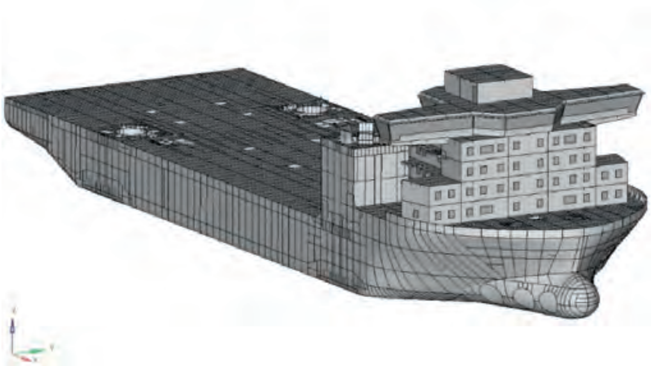

Fig. 2. Global FEM model of jack-up vessel

The numbering convention shown in Fig. 3 was adopted during the calculation and presentation of results. The figure shows an X-type junction; in the case of a T-type junction, the system only consists of subsystems 1, 2 and 3.

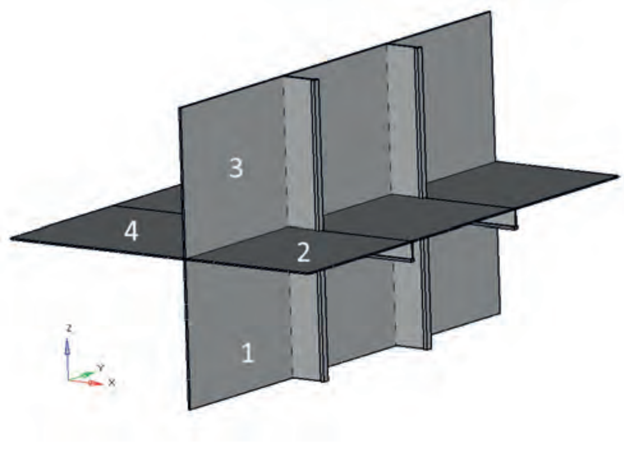

Fig. 3. The numbering convention of subsystems

A typical stiffener spacing of 685 mm was defined in each subsystem. All of the tested systems were made of mild steel and the following material properties were assumed globally: density ρ= 7850 kg/m^3, Poisson's ratio ν=0.3, Young's modulus E=205GPa, and internal damping η=0.04. It was assumed that the value of internal damping is constant and independent from frequency. The assumed value is in the range of values where the DLF had practically no effect on the CLFs of the tested systems. Individual systems are characterised by the following values: connection length (Ly), length of the first (Lz), second (Lx), third (Lz') and fourth (Lx') subsystem, as well as the thickness of the plating of individual subsystems and types of stiffeners. A description of each tested system is provided in Appendix A.

THE FINITE ELEMENTS

A vibroacoustic computation using FEM was carried out with Ansys software. SHELL181 elements were used to model plates and BEAM188 elements were used to model stiffeners. SHELL181 is a four-node element with six degrees of freedom at each node. A BEAM188 element is suitable for analysing slender to moderately stubby/thick beam structures, based on Timoshenko beam theory, which includes shear-deformation effects. Combin14 elements were used as springs on the edges of the submodels.

INPUT POWER AND SUBSYSTEM ENERGY

The outputs obtained from the numerical simulations are the energy and the input power. Energy associated with the out-of-plane vibrations were computed as:

$$E_i = \frac{M<|v_n|^2>}{2} \quad (7)$$

where M is the mass of the subsystem, v_n is the vector of normal velocity, and < > represents the spatial average. The power injected by a single point force is obtained as:

$$P_{in} = \frac{1}{2} Re\{Fv\} \quad (8)$$

where F is the vector of the point force and v is the vector of the velocity at the application spot in the force direction.

LOADS AND BOUNDARY CONDITIONS

Forces were applied to 100 random nodes, at random phases (but at a constant amplitude), to implement a 'rain on the roof' type of load. A new set of random loads was generated for each harmonic solution.

Six springs were attached to each edge node and each of them acted on only one degree of freedom. This made it possible to control individual degrees of freedom. The spring stiffness was calibrated as follows:

- The examined intersection was 'cut out' from the global FEM model, along with the adjacent part of the structure, so that the submodel ended with a primary stiffening member.
- A concentrated force was applied to the joint and the result of the static analysis was obtained in the form of displacements.
- The attached structure was removed from the submodel, springs were created and their stiffnesses were iteratively selected to obtain the same displacements.

For each run of harmonic analysis, 1, 2 or 3 nodes were randomly selected and some of their degrees of freedom were fixed (i.e. locked from translation or translation and rotation). In the rest of this article, such restraints will be called single point constraints (SPC).

THE COMPUTATIONAL WORKFLOW

The entire procedure was programmed in Ansys Parametric Design Language (APDL) and the procedure was as follows:

- Each octave (or third) was represented by seven discrete frequencies.
- N harmonic analyses were performed for each frequency, where N is the number of subsystems.
- For each harmonic analysis, the 'rain on the roof' load on the subsequent subsystem was applied and specific boundary conditions were generated. After each harmonic analysis, the matrices from Eq. (6) were filled in.
- After calculating the CLFs for each frequency, averaging was performed for the entire band. Negative CLFs were not taken into account.
- After calculating the CLFs for all octaves, the boundary condition settings were changed and the next iteration took place. The final result was an average of seven iterations.

VALIDATION METHOD

The method was validated in two ways: by comparing the CLFs with measurements performed by Treszkai et al. [7] and by comparing energy level differences with measurements made by Yin and Hopkins [12]. In the first case, two steel plates without stiffeners (junction #1) were tested while, in the second case, two periodically ribbed Perspex plates (junction #2) were tested. The scheme of the stiffened plates is shown in Fig. 4. The material properties used in both cases are given in Table 1 and the geometrical details are presented in Table 2.

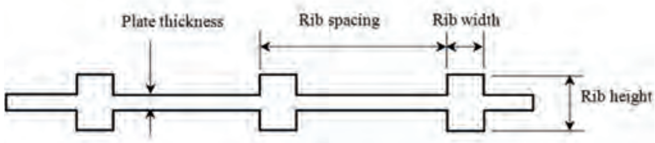

Fig. 4. Periodic ribbed plates scheme. These types of stiffeners were only used for the purposes of comparison with work [12].

Tab. 1. Material properties of the L-junction plates

Junction	Plate	Material	Young's modulus [Pa]	Density [kg/m³]	Poisson's ratio [-]	Internal loss factor [-]
#1	1	Steel	2.05E+11	7850	0.3	0.04
	2	Steel	2.05E+11	7850	0.3	0.04
#2	1	Perspex	4.63E+09	1220	0.3	0.06
	2	Perspex	4.63E+09	1220	0.3	0.06

Tab. 2. Geometrical description of plates

Junction	Plate	Rib orientation to junction line	Plate dimensions [mm]	Rib spacing [mm]	Rib width [mm]	Rib height [mm]
#1	1	N/A	2	N/A	N/A	N/A
	2	N/A	2	N/A	N/A	N/A
#2	1	Perpendicular	10	200	10	60
	2	Parallel	10	100	10	60

RESULTS AND DISCUSSION

VALIDATION

Fig. 5 shows the minimum and maximum values of the CLFs (measured experimentally), FEM/SEA results with a 95% confidence interval and analytically calculated values, based on wave theory for junction #1. The 95% confidence intervals were calculated using the Student's 't' distribution.

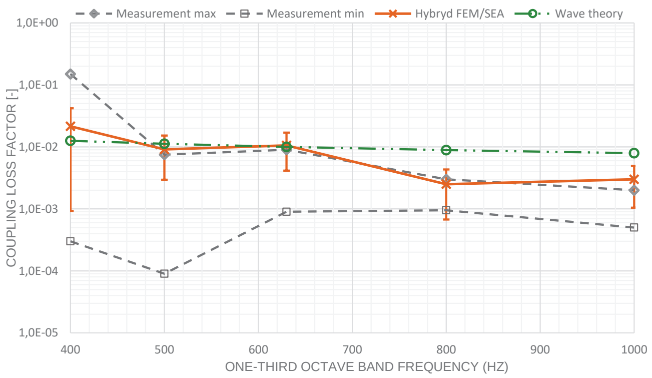

Fig. 5. Junction #1, comparison between hybrid FEM/SEA results, measurements and wave theory prediction.

The graph in Fig. 5 shows a good consistency between hybrid FEM/SEA measurements. As expected, the FEM/SEA values are closer to the maximum measurement results. This could be caused by the fact that the FEM model does not take into account weld imperfections.

The energy level difference (in dB) obtained for junction #2, by hybrid FEM/SEA and the measurements in one-third octave bands, are compared in Fig. 6. Both results are plotted with 95% confidence intervals.

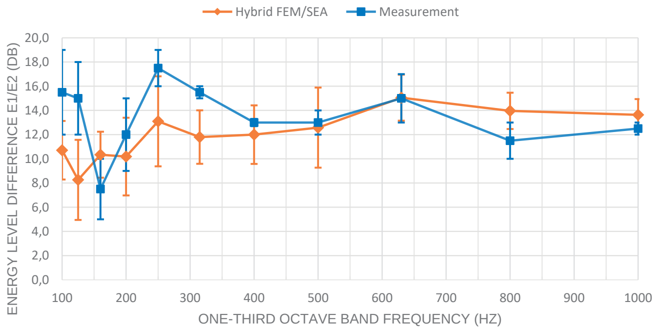

Fig. 6. Junction #2, comparison between hybrid FEM/SEA results and the measurements.

In general, the results can be considered to be acceptably consistent. As expected, larger differences in average values occur in lower frequencies but, in thirds above 300 Hz, the results do not differ by more than 2 dB. Discrepancies for some bands may result from several factors. Firstly, the sampling during the measurements was 1 Hz, while the FEM/SEA result is averaged over seven frequencies for one-third octave. The method of excitation was also different; the rain on the roof' used in FEM simulations is unattainable in the conditions of a real experiment, and so point excitations were used. During the experiment, the boundary conditions did not change. Meanwhile, during the FEM simulation, the stiffness of the model edge restraint changed randomly and random SPCs appeared. This indicates that the ensemble average represents deterministic systems well.

THE INFLUENCE OF THE BOUNDARY CONDITIONS

SEA is used to predict vibration and noise levels at the design stage. One should bear in mind that a shipyard-constructed structure may exhibit variations, compared to the documentation. Sometimes, very small changes can cause a large impact on the subsystems' vibration response, as shown in Figs. 7-8. Fig. 7 shows how the response of the system changes after introducing one more restraint point in a random place on each subsystem. At the statistical energy analysis stage, the stiffness of the connected structure may change and pillars/cutouts may appear. The best solution is to average the random spring stiffness and random SPCs. If any of these unknowns are eliminated, this part of the randomness can be removed from the procedure. In the cases described in this paper, the stiffness of the springs at the edges of the models was randomly selected in the range 70-130% of the mean value.

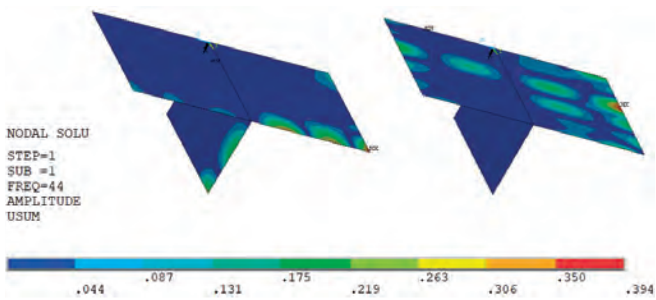

Fig, 7. Displacement graph [mm], result of a steady state harmonic analysis in an exemplary frequency of 44 Hz, at which the influence of irregularity is clearly visible. On the left, there is one single point constraint in a random place for each subsystem. On the right, there are two single point constraints in a random place for each subsystem.

The scatter of CLF values, for one system with seven random boundary conditions, is shown in Fig. 8.

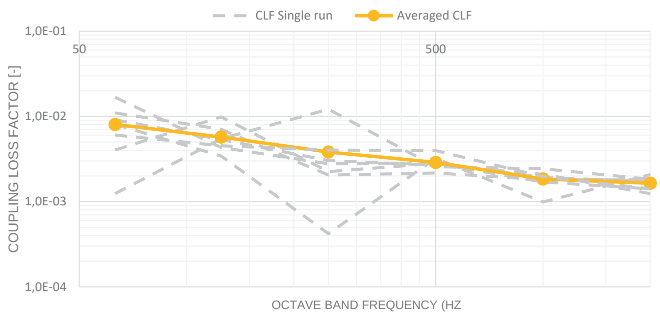

Fig. 8. The coupling loss factors for seven boundary conditions and the averaged value

Fig. 8 shows that a small change in the system can change the CLF value by two orders of magnitude. The dispersion of the results significantly decreases above the 250 Hz octave.

CONCLUSIONS

This paper presents a hybrid FEM/SEA method for estimating the CLF for complex structural joints found on ships. The results obtained with this method were compared to experimental results from two different papers. Acceptably good agreement with the measurement results was achieved. The presented method differs from previous solutions in the following ways:

- The coefficients are averaged in the frequency domain and for various boundary conditions. This allows us to easily reject negative CLFs with minimal impact on the final result.
- By using springs at the edges of the model, the influence of the adjacent structure can be taken into account. Random deviations in spring stiffness allow the result to be obtained more for the ensemble average than for the deterministic case.
- Potential structural discontinuities or additional wave-scattering elements (such as pillars) are introduced into the system as point restraints in random places in the subsystem.
- If the uncertainty associated with any of the above types of boundary conditions disappears, it can be removed from the analysis, making it more deterministic.

Using a hybrid FEM/SEA method, a library of CLFs was created for the structural joints of a jack-up vessel (Appendix A). With the help of this library, one can create many SEA models of vibroacoustic paths on various ships. The presented method is universal and the library can be freely expanded.

ACKNOWLEDGMENTS

This work was performed as a part of the Industrial Doctorate Programme financed by the Polish Ministry of Science and Higher Education. The authors wish to acknowledge the Fem4cad staff in regard to their support for this research.

REFERENCES

1. DNV, “Class documents - Rules for classification, class programmes, class guidelines, offshore standards and statutory interpretations”, 2023. https://www.dnv.com/rules-standards/index.html
2. L. Cremer, M. Heckl, and E.E Ungar, ”Structure-Borne Sound”, Springer-Verlag, New York. 1973.
3. A. Le Bot and V. Cotoni, “Validity diagrams of statistical energy analysis”, Journal of sound and vibration, vol. 329, pp. 221-235, 2010, doi:10.1016/j.jsv.2009.09.008.
4. R.H. Lyon ‘Statistical Energy Analysis of Dynamical Systems: Theory and Applications”, M.I.T. Press. 1975.
5. D.A. Bies and S. Hamid, “In situ determination of loss and coupling factors by the Power Injection Method”, Journal of the Acoustical Society of America, vol.66, 1980, doi: 10.1121/1.2017651.
6. [6] R., Panuszka, J. Wiciak, and M. Iwaniec, “Experimental assessment of coupling loss factors of thin rectangular plates”, Archives of acoustics, vol. 30, pp. 533-551, 2005.
7. M.F. Treszkai, A. Peiffer, and D. Feszty, ”Power Injection Method-based evaluation of the effect of binding technique on the Coupling Loss Factors and Damping Loss Factors in Statistical Energy Analysis simulations”, Manufacturing Technology, vol. 21, pp. 544-558, 2021, doi: 10.21062/mft.2021.065.
8. A.C. Pankaj, S. Sastry, and S.M. Murigendrappa, “A comparison of different methods for determination of

coupling factor and velocity response of coupled plates", Journal of Vibroengineering, vol. 15, pp. 1885-1897, 2013.

9. A.N Thite and B.R. Mace, "Robust estimation of coupling loss factors from finite element analysis", Journal of sound and vibration, vol. 303, pp. 814-831, 2007, doi.org/10.1016/j.jsv.2007.02.004

10. J. Poblet-Puig, "Estimation of the coupling loss factors of structural junctions with in-plane waves by means of the inverse statistical energy analysis problem", Journal of Sound and Vibration, vol. 493, pp. 115850, 2021, doi.org/10.1016/j.jsv.2020.115850.

11. P.J. Shorter and R.S. Langley, "Vibro-acoustic analysis of complex systems", Journal of Sound and Vibration, vol. 288, pp. 669-699, 2005, doi.org/10.1016/j.jsv.2005.07.010.

12. J. Yin and C. Hopkins, "Treating periodic ribbed plates with symmetric ribs as individual subsystems in Statistical Energy Analysis: Models for bending wave transmission across L-junctions in the low- and mid-frequency ranges", Journal of Sound and Vibration, vol. 344, pp.221-241, 2015, http://dx.doi.org/10.1016/j.jsv.2015.01.031.

13. C. Pany, "An Insight on the Estimation of Wave Propagation Constants in an Orthogonal Grid of a Simple Line-Supported Periodic Plate Using a Finite Element Mathematical Model", Frontiers in Mechanical Engineering, vol. 8, p. 926559, 2022, doi.org/10.3389/fmech.2022.926559.

APPENDIX A

Tab. 3 Description of subsystems included in the submodels

	Length [mm]					Thickness [mm]				Stiffener type			
ID	Lx	Ly	Lz	Lx'	Lz'	P1	P2	P3	P4	P1	P2	P3	P4
1	2740	1500	-	-	-	10	10	-	-	FB10x100	HP120x6	-	-
2	2740	1500	-	-	-	20	10	-	-	FB10x100	HP200x9	-	-
3	1500	3500	1950	-	1950	8	10	8	-	HP120x7	FB10x100	HP120x7	-
4	1500	3500	1950	-	1950	20	10	20	-	HP200x9	FB10x100	HP200x9	-
5	1500	2640	1950	-	1950	20	12	20	-	HP200x9	FB10x100	HP200x9	-
6	1500	2640	1950	-	1950	8	12	8	-	HP120x7	FB10x100	HP120x7	-
7	1500	3500	1950	-	1950	9	10	9	-	HP120x6	FB10x100	HP120x6	-
8	1950	2055	3700	-	3100	7	7	7	-	HP120x7	HP100x8	HP120x7	-
9	1950	2055	1500	1950	2400	8	6	8	6	HP160x7	HP80x6	HP160x7	HP80x6
10	1500	3425	1950	2040	1950	8	10	8	8	HP120x7	FB10x100	HP120x7	HP160x7
11	1500	3425	1950	2040	1950	18	18	12	24	HP120x7	FB10x100	HP120x7	HP120x7
12	1500	3425	1950	2040	1950	8	10	8	8	HP120x6	FB10x100	HP120x7	HP160x7
13	1500	3425	1950	2040	1950	8	12	8	8	HP120x6	FB10x100	HP120x7	HP160x7

Table 4 CLF values for selected junctions

ID	Octave	Coupling loss factor [-]											
		1_2	2_1	1_3	2_3	3_2	3_1	1_4	2_4	3_4	4_1	4_2	4_3
1	63	1.2E-01	1.7E-01	-	-	-	-	-	-	-	-	-	-
	125	1.6E-02	1.2E-02	-	-	-	-	-	-	-	-	-	-
	250	1.4E-02	1.2E-02	-	-	-	-	-	-	-	-	-	-
	500	8.1E-03	7.1E-03	-	-	-	-	-	-	-	-	-	-
	1000	7.4E-03	5.8E-03	-	-	-	-	-	-	-	-	-	-
	2000	5.2E-03	4.0E-03	-	-	-	-	-	-	-	-	-	-
2	63	9.5E-03	1.2E-02	-	-	-	-	-	-	-	-	-	-
	125	4.7E-03	6.1E-03	-	-	-	-	-	-	-	-	-	-
	250	3.5E-03	5.7E-03	-	-	-	-	-	-	-	-	-	-
	500	3.6E-03	5.7E-03	-	-	-	-	-	-	-	-	-	-
	1000	3.4E-03	4.7E-03	-	-	-	-	-	-	-	-	-	-
	2000	2.2E-03	3.1E-03	-	-	-	-	-	-	-	-	-	-
3	63	4.1E-03	5.4E-03	2.0E-02	8.0E-03	6.7E-03	1.9E-02	-	-	-	-	-	-
	125	2.5E-03	4.4E-03	3.3E-02	7.7E-03	5.3E-03	3.3E-02	-	-	-	-	-	-
	250	3.2E-03	6.5E-03	6.4E-03	6.5E-03	3.4E-03	6.3E-03	-	-	-	-	-	-
	500	2.8E-03	4.4E-03	4.2E-03	4.4E-03	2.5E-03	4.3E-03	-	-	-	-	-	-
	1000	2.3E-03	4.0E-03	2.2E-03	4.0E-03	2.4E-03	2.2E-03	-	-	-	-	-	-
	2000	1.7E-03	2.8E-03	1.1E-03	2.7E-03	1.8E-03	1.1E-03	-	-	-	-	-	-
4	63	2.6E-03	1.3E-03	7.2E-02	2.4E-03	2.9E-03	5.7E-02	-	-	-	-	-	-
	125	1.3E-03	6.8E-04	6.3E-02	8.0E-04	3.3E-03	6.3E-02	-	-	-	-	-	-
	250	2.1E-03	9.9E-04	3.4E-02	7.4E-04	1.6E-03	3.8E-02	-	-	-	-	-	-
	500	1.7E-03	1.0E-03	1.0E-02	8.5E-04	1.4E-03	1.1E-02	-	-	-	-	-	-
	1000	2.0E-03	1.1E-03	8.5E-03	9.4E-04	1.8E-03	9.2E-03	-	-	-	-	-	-
	2000	1.5E-03	8.4E-04	4.6E-03	7.8E-04	1.5E-03	4.5E-03	-	-	-	-	-	-
5	63	4.8E-02	3.4E-02	4.9E-01	7.2E-03	1.5E-02	3.5E-01	-	-	-	-	-	-
	125	8.1E-03	3.1E-03	7.9E-02	5.9E-03	1.4E-02	1.1E-01	-	-	-	-	-	-
	250	5.7E-03	2.3E-03	3.1E-02	1.9E-03	1.8E-03	2.9E-02	-	-	-	-	-	-
	500	2.0E-03	1.7E-03	1.1E-02	1.6E-03	1.7E-03	1.1E-02	-	-	-	-	-	-
	1000	2.5E-03	1.9E-03	7.0E-03	2.0E-03	2.7E-03	8.2E-03	-	-	-	-	-	-
	2000	2.0E-03	1.3E-03	4.3E-03	1.2E-03	1.8E-03	4.2E-03	-	-	-	-	-	-
6	63	8.5E-03	1.0E-02	1.3E-02	1.7E-02	7.0E-03	1.4E-02	-	-	-	-	-	-
	125	5.9E-03	7.4E-03	7.5E-03	7.9E-03	4.7E-03	1.0E-02	-	-	-	-	-	-
	250	2.4E-03	7.0E-03	4.2E-03	6.4E-03	2.6E-03	3.4E-03	-	-	-	-	-	-
	500	2.6E-03	6.2E-03	3.0E-03	6.5E-03	2.9E-03	3.1E-03	-	-	-	-	-	-
	1000	2.0E-03	4.0E-03	1.6E-03	3.9E-03	2.0E-03	1.7E-03	-	-	-	-	-	-
	2000	1.6E-03	3.0E-03	7.6E-04	3.0E-03	1.7E-03	7.5E-04	-	-	-	-	-	-
7	63	4.6E-03	9.9E-03	2.0E-02	3.3E-03	4.1E-03	1.6E-02	-	-	-	-	-	-
	125	3.6E-03	5.5E-03	1.3E-02	6.4E-03	4.5E-03	1.4E-02	-	-	-	-	-	-
	250	4.3E-03	4.5E-03	6.7E-03	4.3E-03	2.8E-03	7.5E-03	-	-	-	-	-	-
	500	2.7E-03	4.5E-03	5.3E-03	4.5E-03	2.9E-03	5.6E-03	-	-	-	-	-	-
	1000	2.8E-03	4.0E-03	2.7E-03	3.9E-03	2.5E-03	2.5E-03	-	-	-	-	-	-
	2000	1.9E-03	2.7E-03	1.4E-03	2.6E-03	2.0E-03	1.5E-03	-	-	-	-	-	-

ID	Octave	Coupling loss factor [-]											
		1_2	2_1	1_3	2_3	3_2	3_1	1_4	2_4	3_4	4_1	4_2	4_3
8	63	2.6E-03	5.4E-03	7.0E-03	7.7E-03	4.9E-03	1.0E-02	-	-	-	-	-	-
	125	2.3E-03	4.6E-03	3.6E-03	5.1E-03	2.7E-03	4.4E-03	-	-	-	-	-	-
	250	1.9E-03	4.3E-03	2.3E-03	3.2E-03	2.3E-03	4.1E-03	-	-	-	-	-	-
	500	2.1E-03	3.2E-03	1.7E-03	2.9E-03	2.2E-03	2.0E-03	-	-	-	-	-	-
	1000	1.2E-03	2.2E-03	1.0E-03	2.5E-03	1.7E-03	1.2E-03	-	-	-	-	-	-
	2000	7.4E-04	1.3E-03	6.0E-04	1.4E-03	9.2E-04	6.8E-04	-	-	-	-	-	-
9	63	5.0E-03	3.8E-03	3.5E-02	1.3E-03	2.5E-03	2.5E-02	6.7E-03	4.7E-03	1.1E-03	8.6E-04	4.0E-03	2.5E-03
	125	2.0E-03	1.5E-03	1.2E-02	1.3E-03	2.0E-03	6.0E-03	3.2E-03	2.1E-03	1.4E-03	1.6E-03	1.2E-03	1.6E-03
	250	1.9E-03	1.3E-03	7.0E-03	1.3E-03	1.1E-03	4.6E-03	2.2E-03	1.5E-03	1.1E-03	1.1E-03	1.4E-03	1.7E-03
	500	2.4E-03	1.4E-03	4.6E-03	1.3E-03	1.2E-03	2.5E-03	2.5E-03	1.2E-03	1.0E-03	9.2E-04	1.3E-03	1.3E-03
	1000	1.7E-03	9.9E-04	3.3E-03	1.1E-03	1.1E-03	2.2E-03	1.7E-03	9.6E-04	5.6E-04	4.9E-04	1.2E-03	1.0E-03
	2000	1.1E-03	6.1E-04	1.9E-03	6.2E-04	6.2E-04	1.0E-03	1.1E-03	5.6E-04	3.1E-04	2.9E-04	6.6E-04	5.9E-04
10	63	2.5E-03	3.4E-03	9.5E-03	3.9E-03	2.5E-03	8.9E-03	3.5E-03	4.5E-03	6.3E-03	4.2E-03	3.3E-03	4.4E-03
	125	1.5E-03	3.6E-03	8.2E-03	2.9E-03	1.8E-03	8.7E-03	1.9E-03	2.6E-03	4.7E-03	2.8E-03	4.0E-03	4.2E-03
	250	1.9E-03	3.1E-03	2.5E-03	3.3E-03	2.4E-03	2.8E-03	1.3E-03	1.7E-03	6.6E-03	3.4E-03	1.6E-03	2.2E-03
	500	1.5E-03	2.3E-03	1.8E-03	2.4E-03	1.5E-03	2.1E-03	1.0E-03	1.2E-03	3.0E-03	2.4E-03	2.0E-03	2.3E-03
	1000	1.7E-03	2.6E-03	1.3E-03	2.5E-03	1.4E-03	1.1E-03	8.6E-04	1.0E-03	2.0E-03	1.5E-03	1.3E-03	1.7E-03
	2000	1.0E-03	1.8E-03	6.0E-04	1.6E-03	1.0E-03	6.5E-04	5.9E-04	6.6E-04	1.4E-03	9.5E-04	6.9E-04	7.7E-04
11	63	3.1E-03	4.0E-03	2.0E-02	1.5E-03	7.0E-04	1.9E-02	4.8E-02	4.4E-02	8.8E-03	4.7E-03	1.6E-02	7.4E-03
	125	1.7E-03	8.5E-03	9.1E-03	3.0E-03	9.0E-04	6.2E-03	6.1E-02	5.9E-02	4.0E-03	7.6E-03	3.5E-02	4.1E-02
	250	2.4E-03	3.6E-03	2.4E-03	1.6E-03	1.0E-03	2.2E-03	4.0E-03	5.4E-03	3.5E-03	6.0E-03	1.9E-03	4.6E-03
	500	1.5E-03	2.4E-03	8.8E-04	1.0E-03	6.3E-04	5.9E-04	2.4E-03	3.8E-03	3.5E-03	3.4E-03	1.0E-03	2.3E-03
	1000	1.3E-03	1.6E-03	6.4E-04	1.0E-03	4.6E-04	3.4E-04	3.0E-03	3.3E-03	3.0E-03	2.4E-03	9.7E-04	2.0E-03
	2000	1.5E-03	2.1E-03	1.1E-03	1.0E-03	3.9E-04	5.8E-04	2.7E-03	3.3E-03	2.1E-03	1.9E-03	8.2E-04	1.5E-03
12	63	4.0E-03	8.4E-03	8.7E-03	2.0E-02	1.4E-02	5.8E-03	2.7E-03	1.4E-03	7.3E-03	3.2E-03	4.3E-03	8.0E-03
	125	3.2E-03	4.4E-03	4.5E-03	4.3E-03	1.9E-03	4.8E-03	1.3E-03	1.6E-03	5.2E-03	3.3E-03	2.7E-03	2.8E-03
	250	3.0E-03	5.2E-03	1.0E-03	3.9E-03	1.9E-03	7.4E-04	1.9E-03	2.2E-03	4.9E-03	2.2E-03	1.4E-03	2.0E-03
	500	1.8E-03	2.9E-03	8.5E-04	4.4E-03	2.1E-03	7.7E-04	1.4E-03	1.4E-03	2.5E-03	1.3E-03	1.5E-03	1.8E-03
	1000	2.0E-03	3.4E-03	1.1E-03	2.5E-03	1.1E-03	7.9E-04	7.6E-04	7.8E-04	2.2E-03	1.4E-03	1.1E-03	1.4E-03
	2000	1.7E-03	2.8E-03	7.0E-04	2.0E-03	9.9E-04	5.8E-04	5.7E-04	5.5E-04	1.7E-03	8.5E-04	4.7E-04	5.2E-04
13	63	4.0E-03	8.4E-03	8.7E-03	2.0E-02	1.4E-02	5.8E-03	2.7E-03	1.4E-03	7.3E-03	3.2E-03	4.3E-03	8.0E-03
	125	3.2E-03	4.4E-03	4.5E-03	4.3E-03	1.9E-03	4.8E-03	1.3E-03	1.6E-03	5.2E-03	3.3E-03	2.7E-03	2.8E-03
	250	3.0E-03	5.2E-03	1.0E-03	3.9E-03	1.9E-03	7.4E-04	1.9E-03	2.2E-03	4.9E-03	2.2E-03	1.4E-03	2.0E-03
	500	1.8E-03	2.9E-03	8.5E-04	4.4E-03	2.1E-03	7.7E-04	1.4E-03	1.4E-03	2.5E-03	1.3E-03	1.5E-03	1.8E-03
	1000	2.0E-03	3.4E-03	1.1E-03	2.5E-03	1.1E-03	7.9E-04	7.6E-04	7.8E-04	2.2E-03	1.4E-03	1.1E-03	1.4E-03
	2000	1.7E-03	2.8E-03	7.0E-04	2.0E-03	9.9E-04	5.8E-04	5.7E-04	5.5E-04	1.7E-03	8.5E-04	4.7E-04	5.2E-04